A New Discrete Transparent Boundary Condition for Standard and Wide Angle "Parabolic" Equations in Underwater Acoustics[*]

ANTON ARNOLD[1,2] AND MATTHIAS EHRHARDT[1]

[1]Fachbereich Mathematik
TU Berlin, MA 6–2
Straße des 17. Juni 136
D–10623 Berlin, Germany

[2]Center for Applied Mathematics
Purdue University
West Lafayette, IN 47907, USA

E–mail: `arnold@math.tu-berlin.de, ehrhardt@math.tu-berlin.de`

ABSTRACT. This paper is concerned with transparent boundary conditions (TBCs) for standard and wide angle "parabolic" equations (SPE, WAPE) in the application to underwater acoustics (assuming cylindrical symmetry). Existing discretizations of these TBCs have accuracy problems and render the overall Crank–Nicolson finite difference method only conditionally stable. Here, a novel discrete TBC is derived from the discrete whole–space problem that yields an unconditionally stable scheme. The superiority of the new discrete TBC over existing discretizations is illustrated on several benchmark problems.

1. INTRODUCTION

This paper is concerned with a finite difference discretization of *standard* and *wide angle "parabolic" equations.* These models appear as one–way approximations to the Helmholtz equation in cylindrical coordinates with azimuthal symmetry. In particular we will discuss the discretization of transparent boundary conditions.

In the past two decades *"parabolic" equation* (PE) models have been widely used for wave propagation problems in underwater acoustics, where they have been introduced by Tappert [31]. An account on the vast recent literature is given in the survey article [21].

In oceanography one wants to calculate the underwater acoustic pressure $p(z, r)$ emerging from a time–harmonic point source located in the water at $(z_s, 0)$. Here, $r > 0$ denotes the radial range variable and $0 < z < z_b$ the depth variable. The water surface is at $z = 0$, and the sea bottom at $z = z_b$. In our numerical tests of discrete transparent boundary conditions (in §4) we will only deal with horizontal bottoms. However, irregular bottom surfaces and sub–bottom layers can be included by simply extending the range of z. We denote the local sound speed by $c(z, r)$, the density by $\rho(z, r)$, and the attenuation by $\alpha(z, r) \geq 0$. $n(z, r) = c_0/c(z, r)$ is the refractive index, with a reference sound speed c_0 (usually the smallest sound speed in the model). Then the reference wave number is $k_0 = 2\pi f/c_0$, where f denotes the (usually low) frequency of the emitted sound.

The pressure satisfies the Helmholtz equation

$$\frac{1}{r} \frac{\partial}{\partial r} \left(r \frac{\partial p}{\partial r} \right) + \rho \frac{\partial}{\partial z} \left(\rho^{-1} \frac{\partial p}{\partial z} \right) + k_0^2 N^2 p = 0, \qquad r > 0, \tag{1.1}$$

with the complex refractive index

$$N(z, r) = n(z, r) + i\alpha(z, r)/k_0. \tag{1.2}$$

In the far field approximation $(k_0 r \gg 1)$ the (complex valued) outgoing acoustic field

$$\psi(z, r) = \sqrt{k_0 r} \, p(z, r) \, e^{-i k_0 r} \tag{1.3}$$

satisfies the *one–way Helmholtz equation*:

$$\psi_r = i k_0 \big(\sqrt{1 - L} - 1\big) \psi, \qquad r > 0. \tag{1.4}$$

Here, $\sqrt{1 - L}$ is a pseudo–differential operator, and L the Schrödinger operator

$$L = -k_0^{-2} \rho \, \partial_z (\rho^{-1} \partial_z) + V(z, r) \tag{1.5}$$

with the complex valued "potential" $V(z, r) = 1 - N^2(z, r)$.

The evolution equation (1.4) is much easier to solve numerically than the elliptic Helmholtz equation (1.1). Hence, (1.4) forms the basis for all standard linear models in underwater acoustics (normal mode, ray representation, parabolic equation) [2, 31]. Strictly speaking, (1.4) is only valid for horizontally stratified oceans, i.e. for range–independent parameters c, ρ, and α. In practice, however, it is still used in situations with weak range dependence, and backscatter is neglected.

"Parabolic" approximations of (1.4) consist in formally approximating the pseudo–differential operator $\sqrt{1 - L}$ by rational functions of L, which yields a PDE that is easier to discretize than the pseudo–differential equation (1.4). For a detailed description and motivation of this procedure we refer to [11, 16, 17, 21, 31, 32]. The linear approximation of $\sqrt{1 - \lambda}$ by $1 - \frac{\lambda}{2}$ gives the narrow angle or *standard "parabolic" equation* (SPE) of Tappert [31]

$$\psi_r = -\frac{i k_0}{2} L \psi, \qquad r > 0. \tag{1.6}$$

This Schrödinger equation is a reasonable description of waves with a propagation direction within about 15° of the horizontal. Rational approximations of the form

$$(1 - \lambda)^{\frac{1}{2}} \approx f(\lambda) = \frac{p_0 - p_1 \lambda}{1 - q_1 \lambda} \tag{1.7}$$

with real p_0, p_1, q_1 yield the *wide angle "parabolic" equations* (WAPE)

$$\psi_r = i k_0 \left(\frac{p_0 - p_1 L}{1 - q_1 L} - 1 \right) \psi, \qquad r > 0. \tag{1.8}$$

In the sequel we will repeatedly require the condition

$$f'(0) = p_0 q_1 - p_1 < 0. \tag{1.9}$$

With the choice $p_0 = 1$, $p_1 = \frac{3}{4}$, $q_1 = \frac{1}{4}$ ((1,1)–Padé approximant of $(1 - \lambda)^{\frac{1}{2}}$) one obtains the WAPE of Claerbout [10]. In [17] Greene determines these coefficients by minimizing the approximation error of $(1 - \lambda)^{\frac{1}{2}}$ over suitable λ–intervals. These WAPE models furnish a much better description of the wave propagation up to angles of about 40°. Also, higher order analogues of (1.7), (1.8) have been successfully used for acoustic problems [13, 18]. While our strategy to construct discrete transparent boundary conditions (see §3) could be generalized to such cases, we will restrict ourselves here to the WAPE (1.8).

In this article we shall focus on boundary conditions (BC) for the SPE (1.6) and the WAPE (1.8). At the water surface one usually employs a Dirichlet ("pressure release") BC: $\psi(z = 0, r) = 0$. At the sea bottom the wave propagation in water has to be coupled to the wave propagation in the sediments of the bottom. The bottom will be modeled as the homogeneous half–space region $z > z_b$ with constant parameters c_b, ρ_b, and α_b. Throughout this paper we will use a fluid model for the bottom by assuming that (1.8) also holds for $z > z_b$.

In practical simulations one is only interested in the acoustic field $\psi(z, r)$ in the water, i.e. for $0 < z < z_b$. While the physical problem is posed on the unbounded z–interval $(0, \infty)$, one wishes to restrict the computational domain in the z–direction by introducing an artificial boundary at or below the sea bottom. This artificial BC should of course change the model as little as possible. Until recently, the standard strategy was to introduce rather

thick absorbing layers below the sea bottom and then to limit the z–range by again imposing a Dirichlet BC [11, 13, 22, 24, 32]. This, of course, artificially changes the model and it increases the computational costs significantly. In [25] and [27] Papadakis derived *impedance BCs* or *transparent boundary conditions* (TBC) for the SPE and the WAPE, which completely solves the problem of restricting the z–domain without changing the physical model: complementing the WAPE (1.8) with a TBC at z_b allows to recover — on the finite computational domain $(0, z_b)$ — the exact half–space solution on $0 < z < \infty$. As the SPE is a Schrödinger equation, similar strategies have been developed independently for quantum mechanical applications [5, 7, 19].

Towards the end of this introduction we shall now turn to the main motivation of this paper. While TBCs fully solve the problem of cutting off the z–domain for the analytical equation, their numerical discretization is far from trivial. Indeed, all available discretizations suffer from reduced accuracy (in comparison to the discretized half–space problem) and render the overall numerical scheme only conditionally stable [7, 23, 26, 33]. The object of this paper is to construct *discrete transparent boundary conditions* (DTBC) for a Crank–Nicolson finite difference discretization of the WAPE such that the overall scheme is unconditionally stable and as accurate as the discretized half–space problem.

The paper is organized as follows: In §2 we review the TBCs for the SPE and the WAPE. In §3 discrete TBCs are derived and analyzed; their superiority over existing discretizations is illustrated in the numerical tests of §4.

2. Transparent Boundary Conditions and Model Coupling

In this Section we shall first address the well–posedness of the evolution problem for the WAPE in the critical non–dissipative case, i.e. for $\alpha = 0$:

$$\psi_r = ik_0\big[f(L) - 1\big]\psi, \qquad z > 0, \quad r > 0, \tag{2.1}$$

subject to the BC $\psi(0, r) = 0$, and with the rational function f given in (1.7). For simplicity of the analysis we only consider the range–independent situation; for the proof see [6].

Theorem 1. *Assume that the refractive index $n(z)$, the density $\rho(z) > 0$, and $\rho^{-1}(z)$ are bounded for $z > 0$. Then, the WAPE has a unique solution for all initial data in the weighted L^2–space $L^2(\mathbb{R}^+; \rho^{-1}dz)$ if and only if the pole of $f(\lambda)$ at $\tilde{\lambda} = q_1^{-1}$ is not an eigenvalue of the operator L with Dirichlet BCs at $z = 0$.*

In applications of underwater acoustics the sound speed $c(z)$ is typically larger in the sea bottom than in the water. Therefore $V(z)$ forms a "potential well" in the water region $0 < z < z_b$, which typically gives rise to bound states of L that represent the propagating modes of (1.4) and (1.8). All of the corresponding eigenvalues satisfy $0 < \lambda_j < V_b = 1 - c_0^2/c_b^2 < 1$, if $c_0 = \min_{z>0} c(z)$. As q_1 is much smaller than 1 in all practical simulations ($\frac{1}{4}$ in the WAPE of Claerbout; also cf. [17]), $\tilde{\lambda}$ usually lies in $[V_b, \infty)$, the continuous spectrum of L. Theorem 1 then guarantees the unique solvability of the evolution equation (2.1) for any initial data. Let us compare the situation at hand (i.e. the WAPE on the original unbounded interval — and later also the WAPE with a TBC) to the WAPE restricted to a finite z–interval with absorbing layers: there, L has a pure eigenvalue spectrum which inhibits the solvability of (2.1) in several cases of practical relevance [3].

Now we turn to the matching conditions and later the TBCs at the water–bottom interface ($z = z_b$). As the density is typically discontinuous there, one requires continuity of the pressure and the normal particle velocity:

$$\psi(z_b-, r) = \psi(z_b+, r), \tag{2.2a}$$

$$\frac{\psi_z(z_b-, r)}{\rho_w} = \frac{\psi_z(z_b+, r)}{\rho_b}, \tag{2.2b}$$

where $\rho_w = \rho(z_b-, r)$ is the water density just above the bottom and ρ_b denotes the constant density of the bottom.

With these matching conditions one can easily derive an estimate for the L^2–decay of solutions to the WAPE (1.8), $z > 0$. We assume $\rho = \rho(z)$ and apply the operator $1 - q_1 L$ to (1.8):

$$\left[1 - q_1 V + q_1 k_0^{-2}\rho\,\partial_z(\rho^{-1}\partial_z)\right]\psi_r$$
$$= ik_0\left[p_0 - 1 - (p_1 - q_1)V + (p_1 - q_1)k_0^{-2}\rho\,\partial_z(\rho^{-1}\partial_z)\right]\psi. \quad (2.3)$$

A standard procedure (multiplying (2.3) by $\bar{\psi}\rho^{-1}$, integrating by parts on $0 < z < z_b$, and taking the real part, and an analogous procedure for (2.3) multiplied by $\bar{\psi}_r\rho^{-1}$) eventually gives

$$\partial_r\|\psi(.,r)\|^2 = -2C_1\int_0^\infty \alpha\,\frac{c_0}{c}\left|\tilde{\partial}_r\psi\right|^2\rho^{-1}\,dz, \quad C_1 = \frac{2(p_1 - q_1)^2}{p_1 - p_0 q_1}, \quad (2.4)$$

for the weighted L^2–norm

$$\|\psi(.,r)\|^2 = \int_0^\infty |\psi(z,r)|^2\,\rho^{-1}(z)\,dz. \quad (2.5)$$

In the dissipation–free case ($\alpha \equiv 0$) $\|\psi(.,r)\|$ is conserved and for $\alpha > 0$ and $p_0 q_1 - p_1 < 0$ it decays. The discrete analogue of this "energy"–conservation (or –decay for $\alpha > 0$) will be the main ingredient for showing unconditional stability of the finite difference scheme in §3.

Now we shall review the transparent bottom boundary condition for the SPE and sketch the derivation of the TBC for the WAPE. We assume that the initial data $\psi^I = \psi(z, 0)$, which models a point source located at $(z_s, 0)$, is supported in $0 < z < z_b$. Also, let the bottom region be homogenous, i.e. all physical parameters be constant for $z > z_b$. The basic idea of the derivation is to explicitly solve the equation in the bottom region, which is the exterior of the computational domain $(0, z_b)$. The TBC for the SPE (or Schrödinger equation) was derived in [5, 7, 19, 23, 25, 27] for various application fields:

$$\psi(z_b, r) = -(2\pi k_0)^{-\frac{1}{2}}\,e^{\frac{\pi}{4}i}\,\frac{\rho_b}{\rho_w}\int_0^r \psi_z(z_b, r - \tau)\,e^{ib\tau}\tau^{-\frac{1}{2}}\,d\tau, \quad (2.6)$$

with $b = k_0(N_b^2 - 1)/2$. This BC is nonlocal in the range variable r and involves a mildly singular convolution kernel. Equivalently, it can be written as

$$\psi_z(z_b, r) = -\left(\frac{2k_0}{\pi}\right)^{\frac{1}{2}}e^{-\frac{\pi}{4}i}\,e^{ibr}\,\frac{\rho_w}{\rho_b}\,\frac{d}{dr}\int_0^r \psi(z_b, \tau)\,e^{-ib\tau}(r - \tau)^{-\frac{1}{2}}\,d\tau. \quad (2.7)$$

In order to derive the TBC for the WAPE we consider (2.3) in the bottom region:

$$(\delta_b + q_1 k_0^{-2}\partial_z^2)\psi_r = i\left[\upsilon_b + (p_1 - q_1)k_0^{-1}\partial_z^2\right]\psi, \qquad z > z_b, \quad (2.8)$$

with

$$\delta_b = 1 - q_1(1 - N_b^2), \quad \upsilon_b = k_0\left[p_0 - 1 - (p_1 - q_1)(1 - N_b^2)\right].$$

After a Laplace transformation of (2.8) in r we get

$$\left[q_1 s - i(p_1 - q_1)k_0\right]\hat{\psi}_{zz}(z, s) = k_0^2(i\upsilon_b - \delta_b s)\hat{\psi}(z, s). \quad (2.9)$$

Since its solution has to decay as $z \to \infty$ we obtain

$$\hat{\psi}(z, s) = \hat{\psi}(z_b+, s)\exp\left\{-k_0\sqrt[+]{\frac{i\upsilon_b - \delta_b s}{q_1 s - i(p_1 - q_1)k_0}}\,(z - z_b)\right\}, \quad z > z_b, \quad (2.10)$$

and with the matching conditions (2.2) this gives

$$\hat{\psi}_z(z_b-, s) = -k_0\frac{\rho_w}{\rho_b}\sqrt[+]{\frac{i\upsilon_b - \delta_b s}{q_1 s - i(p_1 - q_1)k_0}}\,\hat{\psi}(z_b-, s). \quad (2.11)$$

4

Here, $\sqrt[+]{}$ denotes the branch of the square root with nonnegative real part. An inverse Laplace transformation [8] yields the TBC at the bottom for the WAPE:

$$\psi(z_b, r) = -i\eta\,\frac{\rho_b}{\rho_w}\,\psi_z(z_b, r)$$

$$+ \beta\,\eta\,\frac{\rho_b}{\rho_w}\int_0^r \psi_z(z_b, r-\tau)\,e^{i\theta\tau}e^{i\beta\tau}\big[J_0(\beta\tau) + iJ_1(\beta\tau)\big]\,d\tau, \quad (2.12)$$

$$\eta = \frac{1}{k_0}\sqrt[+]{\frac{q_1}{\delta_b}}, \quad \beta = -\frac{p_1 - p_0 q_1}{2\,q_1}\frac{k_0}{\delta_b}, \quad \theta = \frac{p_1 - q_1}{q_1}\,k_0,$$

where J_0, J_1 denote the Bessel functions of order 0 and 1, respectively. This is a slight generalization of the TBC derived in [27] where p_0 was equal to 1. Equivalently, (2.12) can be written as

$$\psi_z(z_b, r) = i\eta^{-1}\frac{\rho_w}{\rho_b}\,\psi(z_b, r)$$

$$+ \beta\,\eta^{-1}\frac{\rho_w}{\rho_b}\int_0^r \psi(z_b, r-\tau)\,e^{i\theta\tau}e^{i\beta\tau}\big[J_0(\beta\tau) - iJ_1(\beta\tau)\big]\,d\tau. \quad (2.13)$$

Both TBCs are non–local in r; in range marching algorithms they thus require to store the bottom boundary data of all previous range levels.

We remark that the asymptotic behaviour (for $r \to \infty$) of the convolution kernel in the TBC (2.7) is $O(r^{-3/2})$, which can be seen after an integration by parts. Using the asymptotic behaviour of the Bessel functions (see (3.5)) one finds that the convolution kernel of (2.13) also decays like $O(r^{-3/2})$.

3. Discrete Transparent Boundary Conditions

In this Section we shall discuss how to discretize the TBCs (2.6), (2.12) in conjunction with a Crank–Nicolson finite difference scheme for the SPE and the WAPE.

With the uniform grid points $z_j = jh$, $r_n = nk$ ($h = \Delta z$, $k = \Delta r$) and the approximation $\psi_j^n \sim \psi(z_j, r_n)$ the discretized WAPE (2.3) reads:

$$\big[1 - q_1 V_j^{n+\frac{1}{2}} + q_1 k_0^{-2}\rho_j D_{\frac{h}{2}}^0(\rho_j^{-1}D_{\frac{h}{2}}^0)\big]D_k^+\psi_j^n$$

$$= ik_0\big[p_0 - 1 - (p_1 - q_1)V_j^{n+\frac{1}{2}} + (p_1 - q_1)k_0^{-2}\rho_j D_{\frac{h}{2}}^0(\rho_j^{-1}D_{\frac{h}{2}}^0)\big]\frac{\psi_j^n + \psi_j^{n+1}}{2}, \quad (3.1)$$

with $V_j^{n+\frac{1}{2}} := V(z_j, r_{n+\frac{1}{2}})$ and the usual difference operators

$$D_k^+\psi_j^n = \frac{\psi_j^{n+1} - \psi_j^n}{k}, \qquad D_{\frac{h}{2}}^0\psi_j^n = \frac{\psi_{j+\frac{1}{2}}^n - \psi_{j-\frac{1}{2}}^n}{h}.$$

It is well known that this scheme is second order in h and k and unconditionally stable [3]. Proceeding similarly to the derivation of (2.4) one can show

$$D_k^+ \sum_{j\in\mathbb{Z}}\frac{|\psi_j^n|^2}{\rho_j} = -C_1 k_0^{-1}\sum_{j\in\mathbb{Z}}\text{Im}\left\{V_j^{n+\frac{1}{2}}\right\}\left|\psi_j^{n+\frac{1}{2}} + \frac{iq_1}{p_1 - q_1}k_0^{-1}D_k^+\psi_j^n\right|^2\frac{1}{\rho_j}, \quad (3.2)$$

with $C_1 = 2(p_1 - q_1)^2/(p_1 - p_0 q_1)$. Hence, the scheme (3.1) preserves the discrete weighted L^2–norm in the dissipation–free case (V real). This also holds when using a homogeneous Dirichlet BC at $j = 0$.

We shall now compare two strategies to discretize TBCs. First we review a known discretization from the literature, where the analytic TBC (2.6) at $z_b = Jh$ was discretized in an *ad–hoc fashion*. In [33] Thomson and Mayfield used the following *discretized TBC* for the SPE:

$$\psi_J^n - \psi_{J-1}^n = \frac{h}{2Bk^{\frac{1}{2}}}\psi_J^n - B'\sum_{m=1}^{n-1}(\psi_J^{n-m} - \psi_{J-1}^{n-m})\hat{\ell}_m, \quad (3.3)$$

5

with

$$B = -(2\pi k_0)^{-\frac{1}{2}} e^{\frac{\pi}{4}i} \frac{\rho_b}{\rho_w}, \quad B' = e^{\frac{i}{2}bk} \frac{\sin(\frac{1}{2}bk)}{\frac{1}{2}bk}, \quad \hat{\ell}_m = \frac{e^{ibmk}}{2\sqrt{m + \frac{1}{2}}}.$$

To illustrate the problems of this discretization strategy numerically, we shall also use an analogous discretization of the TBC (2.12) for the WAPE:

$$\int_0^r \psi_z(z_b, r_n - \tau) \, e^{i\theta\tau} e^{i\beta\tau} \left[J_0(\beta\tau) + i J_1(\beta\tau) \right] d\tau$$

$$= \sum_{m=0}^{n-1} \int_{r_m}^{r_{m+1}} \psi_z(z_b, r_n - \tau) \, e^{i\theta\tau} \left[\widetilde{J}_0(\beta\tau) + i \widetilde{J}_1(\beta\tau) \right] d\tau$$

$$\approx \sum_{m=0}^{n-1} \frac{\psi_J^{n-m} - \psi_{J-1}^{n-m}}{h} \left[\widetilde{J}_0(\beta r_{m+\frac{1}{2}}) + i \widetilde{J}_1(\beta r_{m+\frac{1}{2}}) \right] \int_{r_m}^{r_{m+1}} e^{i\theta\tau} \, d\tau,$$

with the *damped Bessel functions* $\widetilde{J}_\nu(z) := e^{iz} J_\nu(z)$, $z \in \mathbb{C}$. This yields the following discretized TBC:

$$\psi_J^n - \psi_{J-1}^n = \frac{ih}{\eta} \frac{\rho_w}{\rho_b} \psi_J^n - B' \sum_{m=0}^{n-1} \left(\psi_J^{n-m} - \psi_{J-1}^{n-m} \right) \tilde{\ell}_m, \qquad (3.4)$$

with

$$B' = i\beta \, e^{\frac{i}{2}\theta k} \frac{\sin(\frac{1}{2}\theta k)}{\frac{1}{2}\theta}, \quad \tilde{\ell}_m = e^{i\theta mk} \left[\widetilde{J}_0(\beta r_{m+\frac{1}{2}}) + i \widetilde{J}_1(\beta r_{m+\frac{1}{2}}) \right].$$

In far field simulations one has to evaluate $J_\nu(z)$ for large complex z, when numerically calculating these convolution coefficients $\tilde{\ell}_n$. This, however, is a rather delicate problem, and many standard software routines are not able to evaluate $J_\nu(z)$ for large complex z. This is due to the exponential growth of the Bessel functions for fixed ν and $|z| \to \infty$ (see [1]):

$$J_\nu(z) = \left(\frac{2}{\pi z} \right)^{\frac{1}{2}} \left\{ \cos\left(z - \nu\frac{\pi}{2} - \frac{\pi}{4} \right) + e^{|\mathrm{Im}\, z|} \, \mathrm{O}\big(|z|^{-1}\big) \right\}, \quad -\pi < \arg z < \pi. \qquad (3.5)$$

For this reason we used a subroutine of Amos [4] to evaluate the damped Bessel functions $\widetilde{J}_\nu(z)$, $\mathrm{Im}\, z \geq 0$ (note that $\mathrm{Im}\, \beta \geq 0$ for the standard parameter choices in (1.7): $p_1 - p_0 q_1 > 0$ and $q_1 > 0$).

In [23] Mayfield showed that the *discretized TBC* for the SPE (3.3) destroys the unconditional stability of the underlying Crank–Nicolson scheme and one can expect a similar behaviour for the WAPE. Another problem of these existing discretizations is that they induce numerical reflections at the boundary, particularly when using coarse grids. Hence, the existing *discretized TBC* suffers from both stability problems and reduced accuracy, which therefore requires the usage of unnecessarily fine grids.

Instead of using an ad–hoc discretization of the analytic TBCs like (3.3) or (3.4) we will construct *discrete TBCs* of the fully discretized half–space problem. Our new strategy solves both problems of the *discretized TBC* at no additional computational costs. The resulting DTBC is a generalization of the DTBC for the Schrödinger equation in [5]. The same strategy was used in [15] for advection diffusion equations and in [14] for the wave equation in the frequency domain. With our DTBC the numerical solution on the computational domain $0 \leq j \leq J$ exactly equals the discrete half–space solution (on $j \in \mathbb{N}_0$) restricted to the computational domain $0 \leq j \leq J$. Therefore, our overall scheme inherits the unconditional stability of the half–space solution that is implied by the discrete L^2–estimate (3.2).

To derive the DTBC we will now mimic the derivation of the analytic TBCs from §2 on a discrete level. For the initial data we assume $\psi_j^0 = 0$, $j \geq J - 1$ and solve the discrete

exterior problem in the bottom region, i.e. the Crank–Nicolson finite difference scheme (3.1) for $j \geq J$:

$$\left[R\delta_b + q\Delta_h^2\right](\psi_j^{n+1} - \psi_j^n) = i\left[R\kappa_b + \Delta_h^2\right](\psi_j^{n+1} + \psi_j^n), \tag{3.6}$$

with

$$\delta_b = 1 - q_1(1 - N_b^2), \quad R = \frac{2k_0}{p_1 - q_1}\frac{h^2}{k}, \quad q = \frac{k}{2}\frac{q_1}{p_1 - q_1}k_0^{-1},$$

$$\kappa_b = \frac{k}{2}k_0\left[p_0 - 1 - (p_1 - q_1)(1 - N_b^2)\right],$$

where $\Delta_h^2\psi_j^n = \psi_{j+1}^n - 2\psi_j^n + \psi_{j-1}^n$, and R is proportional to the parabolic mesh ratio. By using the Z–transform:

$$\mathcal{Z}\{\psi_j^n\} = \hat{\psi}_j(z) := \sum_{n=0}^{\infty} \psi_j^n\, z^{-n}, \quad z \in \mathbb{C}, \quad |z| > 1, \tag{3.7}$$

(3.6) is transformed to

$$\left[z + 1 + iq(z-1)\right]\Delta_h^2\hat{\psi}_j(z) = -iR\left[\delta_b(z-1) - i\kappa_b(z+1)\right]\hat{\psi}_j(z). \tag{3.8}$$

The solution of the resulting second order difference equation takes the form $\hat{\psi}_j(z) = \nu_1^j(z)$, $j \geq J$, where $\nu_1(z)$ solves

$$\nu^2 - 2\left[1 - \frac{iR}{2}\frac{\delta_b(z-1) - i\kappa_b(z+1)}{z + 1 + iq(z-1)}\right]\nu + 1 = 0. \tag{3.9}$$

For the decreasing mode (as $j \to \infty$) we require $|\nu_1(z)| < 1$. We obtain the Z–transformed DTBC as

$$\hat{\psi}_{J-1}(z) = \nu_1^{-1}(z)\,\hat{\psi}_J(z), \tag{3.10}$$

and in a tedious calculation this can be inverse transformed explicitly. The DTBC for the SPE and the WAPE then reads:

$$(1 + iq)\,\psi_{J-1}^n = \psi_J^n * \ell_n = \sum_{m=1}^{n} \psi_J^m\, \ell_{n-m}, \quad n \geq 1, \tag{3.11}$$

with the convolution coefficients $\ell_n := (1 + iq)\mathcal{Z}^{-1}\{\nu_1^{-1}(z)\}$ given by

$$\begin{aligned}
\ell_n = {}&\left[1 + iq + \frac{i}{2}(\gamma - i\sigma)e^{-i\xi}\right]\delta_n^0 - \frac{i}{2}H(-1)^n e^{in\xi} \\
&- \zeta\left\{Q_n(\mu) + e^{-i\xi}\lambda^{-2}Q_{n-1}(\mu) + \omega e^{-i\varphi}\sum_{m=0}^{n-1}(-e^{i\xi})^{n-m}Q_m(\mu)\right\},
\end{aligned} \tag{3.12}$$

$$\gamma = R\,\delta_b, \quad \sigma = -R\,\kappa_b, \quad \lambda = \sqrt[\dagger]{\frac{E}{G}}, \quad \mu = \frac{F}{\sqrt[4]{EG}}, \quad \omega = \frac{H^2}{|E|},$$

$$\xi = \arg\frac{1 - iq}{1 + iq}, \quad \varphi = \arg E, \quad \zeta = \frac{i}{2}|E|^{\frac{1}{2}}e^{i\frac{\varphi}{2}},$$

$$E = (\gamma + i\sigma)\left[\gamma - 4q + i(\sigma + 4)\right], \quad F = \gamma(\gamma - 4q) + \sigma(\sigma + 4),$$

$$G = (\gamma - i\sigma)\left[\gamma - 4q - i(\sigma + 4)\right], \quad H = \gamma + i\sigma + (\gamma - i\sigma)e^{-i\xi}.$$

In (3.12) δ_n^0 denotes the Kronecker symbol and $Q_n(\mu) := \lambda^{-n}P_n(\mu)$ the *damped Legendre polynomials* ($Q_0 \equiv 1$, $Q_{-1} \equiv 0$). In the non–dissipative case ($\alpha_b = 0$) we have $|\lambda| = 1$, $\mu \in [-1, 1]$, and hence $|P_n(\mu)| \leq 1$. In the dissipative case $\alpha_b > 0$ we have $|\lambda| > 1$, μ becomes complex and $|P_n(\mu)|$ typically grows with n. In order to evaluate ℓ_n in a numerically stable fashion it is therefore necessary to use the damped polynomials $Q_n(\mu)$ in (3.12).

The convolution coefficients (3.12) behave asymptotically as

$$\ell_n \cong -iH(-1)^n e^{in\xi}, \quad n \to \infty, \tag{3.13}$$

7

which may lead to subtractive cancellation in (3.11) (note that $\psi_J^m \approx \psi_J^{m+1}$ in a reasonable discretization). Therefore we use the following numerically more stable fashion of the DTBC in the implementation:

$$(1 + iq)\,\psi_{J-1}^n - \ell_0\,\psi_J^n = (1 - iq)\,\psi_{J-1}^{n-1} + \sum_{m=1}^{n-1} \psi_J^m\, s_{n-m}, \qquad (3.14)$$

with $s_n := \ell_n + e^{i\xi}\ell_{n-1}$, $n \geq 1$. The coefficients s_n are calculated as

$$s_n = \left[(1 + iq)e^{i\xi} + \frac{i}{2}(\gamma - i\sigma)\right]\delta_n^1 + \zeta\,\frac{Q_n(\mu) - \lambda^{-2}Q_{n-2}(\mu)}{2n - 1}. \qquad (3.15)$$

Alternatively, they can be calculated directly with the recurrence formula

$$s_n = \frac{2n - 3}{n}\mu\lambda^{-1}s_{n-1} - \frac{n - 3}{n}\lambda^{-2}s_{n-2}, \quad n \geq 4, \qquad (3.16)$$

once s_1, s_2, s_3 are computed from (3.15). Using asymptotic properties of the Legendre polynomials [30] one finds $s_n = O(n^{-3/2})$, $n \to \infty$ which agrees with the decay of the convolution kernel in the differential TBCs (2.6), (2.12).

This decay of the s_n motivates to consider also a simplified version of the DTBC (3.14) with the convolution coefficients being cut off beyond an index M, i.e. to only consider the "recent past" in the convolution in (3.14).

So far we did not consider the (typical) density jump at the sea bottom in the DTBC (3.11). In the following we review two possible discretizations of the water–bottom interface. For the usual grid z_j, $j \in \mathbb{N}_0$ with $Jh = z_b$ the discontinuity of ρ is located at the grid point z_J. In this case it is a standard practice [3, 24] to use (3.1) with

$$\rho_j = \begin{cases} \rho_w, & j < J, \\ \frac{2\,\rho_b\rho_w}{\rho_b + \rho_w}, & j = J, \\ \rho_b, & j > J. \end{cases} \qquad (3.17)$$

As an alternative one may use an offset grid, i.e. $\tilde{z}_j = (j + \frac{1}{2})h$, $\tilde{\psi}_j^n \sim \psi(\tilde{z}_j, r_n)$, $j = -1(1)J$, where the water–bottom interface with the density jump lies between the grid points $j = J-1$ and J. For discretizing the matching conditions in this case one wants to find suitable approximations for ψ and ρ at the interface z_b, $\Psi \sim \psi(z_b)$ and $\rho_{eff} = \rho(z_b)$, such that both sides of the discretized second matching condition (2.2b)

$$\frac{1}{\rho_w}\frac{\tilde{\psi}_J^n - \Psi}{h/2} = \frac{1}{\rho_b}\frac{\Psi - \tilde{\psi}_{J-1}^n}{h/2} \quad \text{are equal to} \quad \frac{1}{\rho_{eff}}\frac{\tilde{\psi}_J^n - \tilde{\psi}_{J-1}^n}{h}. \qquad (3.18)$$

This approach results in an *effective density* $\rho_{eff} = (\rho_w + \rho_b)/2$ (based on a different derivation this was also used in [12]). In numerical tests we found that the offset grid with the above choice of ρ_{eff} produces slightly better results that have less Gibbs' oscillations at the discontinuity of ψ_z at z_b. This may be understood by the fact that (3.17) requires a higher order derivation (using the evolution equation) than our derivation (3.18) (see also [12, 22, 24]). Because of the discontinuity of ψ_z the higher order derivation yields (slightly) poorer results. Therefore we choose the offset grid for the implementation of the DTBC. At the surface we use instead of $\psi_0^n = 0$ the offset BC $\tilde{\psi}_0^n = -\tilde{\psi}_{-1}^n$.

Finally it remains to reformulate the DTBC (3.11) such that the density jump is taken into account. We rewrite the discretization of the second depth derivative at $j = J$ from (3.1):

$$h^2\left[\rho_J\ D_{\frac{h}{2}}^0\left(\rho_J^{-1}D_{\frac{h}{2}}^0\tilde{\psi}_J^n\right)\right] = \Delta_h^2\tilde{\psi}_J^n + \left(1 - \frac{\rho_b}{\rho_{eff}}\right)\left(\tilde{\psi}_J^n - \tilde{\psi}_{J-1}^n\right). \qquad (3.19)$$

Comparing the r.h.s. of (3.19) to (3.6) we observe that only one additional term appears, and instead of (3.8) we get

$$\hat{\tilde{\psi}}_{J+1}(z) - \left[1 - iR\frac{\delta_b(z-1) - i\kappa_b(z+1)}{z + 1 + iq(z-1)}\right]\hat{\tilde{\psi}}_J(z) = \frac{\rho_b}{\rho_{eff}}\left(\hat{\tilde{\psi}}_J(z) - \hat{\tilde{\psi}}_{J-1}(z)\right). \qquad (3.20)$$

8

Using $\hat{\tilde{\psi}}_{J+1}(z) = \nu_1(z)\,\hat{\tilde{\psi}}_J(z)$, where $\nu_1(z)$ denotes the solution of (3.9), and considering the fact that $\nu_1(z) + \nu_1^{-1}(z)$ is equal to the term in the squared brackets in (3.20) we obtain the Z–transformed DTBC:

$$\hat{\tilde{\psi}}_J(z) - \hat{\tilde{\psi}}_{J-1}(z) = \frac{\rho_{eff}}{\rho_b}\,\hat{\tilde{\psi}}_J(z) - \frac{\rho_{eff}}{\rho_b}\,\nu_1^{-1}(z)\hat{\tilde{\psi}}_J(z). \qquad (3.21)$$

Hence, the DTBC including the density jump reads

$$(1 + iq)\,\frac{\rho_b}{\rho_{eff}}\,\tilde{\psi}_{J-1}^n + \Big[(1 + iq)\big(1 - \frac{\rho_b}{\rho_{eff}}\big) - \ell_0\Big]\tilde{\psi}_J^n$$

$$= -(1 - iq)\,\frac{\rho_b}{\rho_{eff}}\,\tilde{\psi}_{J-1}^{n-1} - (1 - iq)\big(1 - \frac{\rho_b}{\rho_{eff}}\big)\tilde{\psi}_J^{n-1} + \sum_{m=1}^{n-1} \tilde{\psi}_J^m\, s_{n-m}, \quad (3.22)$$

with the convolution coefficients s_n given by (3.15).

4. Numerical Examples

In the following examples of this Section we shall compare the numerical result from using our new discrete TBC to the solution using the discretized TBC of Thomson and Mayfield [33] for both the SPE and the WAPE. Due to its construction, our DTBC yields exactly (up to round–off errors) the numerical half–space solution restricted to the computational interval $[0, z_b]$. The simulation with discretized TBCs requires the same numerical effort. However, their solution may (on coarse grids) strongly deviate from the half–space solution.

In each example we used the Gaussian beam from [21] as initial data. Below we present the transmission loss $-10\log_{10}|p|^2$, where the acoustic pressure p is calculated from (1.3).

Example 1. This is a well–known benchmark problem from the literature [21, 27, 33]. In this example the ocean region ($0 < z < 240\,\mathrm{m}$) with the uniform density $\rho_w = 1.0\,\mathrm{gcm}^{-3}$ is modeled by the SPE (1.6). It contains no attenuation and a large density jump ($\rho_b = 2.1\,\mathrm{gcm}^{-3}$) at the water–bottom interface. Hence, this problem provides a test of the treatment of the density jump in the TBCs applied along $z_b = 240\,\mathrm{m}$.

The source of $f = 100\,\mathrm{Hz}$ is located at a water depth $z_s = 30\,\mathrm{m}$ and the receiver depth is at $z_r = 90\,\mathrm{m}$. The sound speed profile in water is given by $c(z) = 1498 + |120 - z|/60\,\mathrm{ms}^{-1}$, and the sound speed in the bottom is $c_b = 1505\,\mathrm{ms}^{-1}$. For our calculations up to a maximum range of $20\,\mathrm{km}$ we used a reference sound speed $c_0 = 1500\,\mathrm{ms}^{-1}$ and a computational grid with depth step $\Delta z = 2\,\mathrm{m}$ and range step $\Delta r = 5\,\mathrm{m}$ (the same step sizes were used in [33]).

In Figure 1 the solid line is the solution with our new discrete TBC (3.22) and the dotted line is obtained with the discretized TBC (3.3). The discretized TBC clearly introduces a systematic phase–shift error, which is roughly proportional to Δz. The discretized TBC also produces artificial oscillations (cf. the zoomed region), while our new DTBC yields the smooth solution with the same numerical effort.

Figure 2 shows the poor agreement of the solution using the discretized TBC with the computed half–space solution, which coincides with the solution using our new DTBC.

Example 2. This example appeared as the NORDA test case 3B in the PE Workshop I [20, 21, 27, 33]. The environment for this example consists of an isovelocity water column ($c(z) = 1500\,\mathrm{ms}^{-1}$) over an isovelocity half–space bottom ($c_b = 1590\,\mathrm{ms}^{-1}$). The density changes at $z_b = 100\,\mathrm{m}$ from $\rho_w = 1.0\,\mathrm{gcm}^{-3}$ in the water to $\rho_b = 1.2\,\mathrm{gcm}^{-3}$ in the bottom. The source and the receiver are located at the same depth near the bottom: $z_s = z_r = 99.5\,\mathrm{m}$. The source frequency is $f = 250\,\mathrm{Hz}$. The attenuation in the water is zero, and the bottom attenuation is $\alpha_b = 0.5\,\mathrm{dB}/\lambda_b$, where $\lambda_b = c_b/f$ denotes the wavelength of sound in the bottom. Here, the steepest angle of propagation (which is the equivalent ray–angle of the highest of the 11 propagating modes) is approximately $20°$ (cf. [20, 33]). Since the source is located near the bottom, the higher modes are significantly excited. Therefore the wide angle capability is important here and we use the WAPE (1.8) (with the coefficients of Claerbout) to solve this benchmark problem.
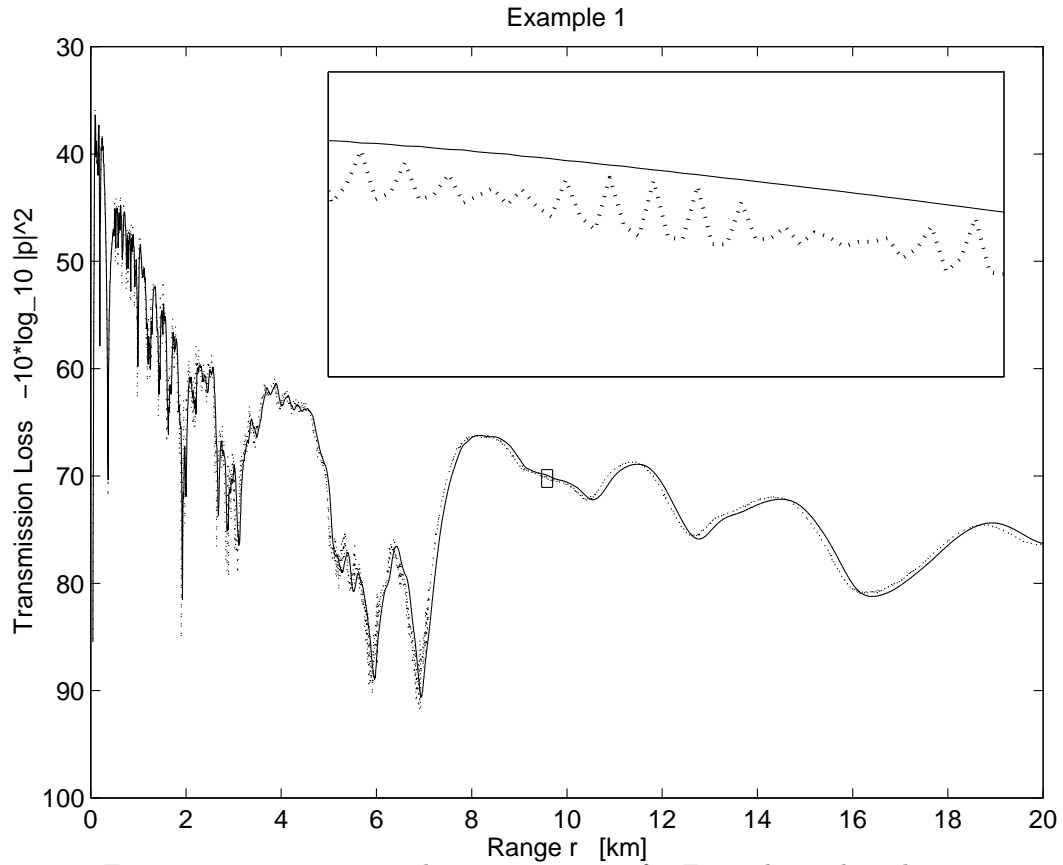
FIGURE 1. Transmission loss at $z_r = 90\,\mathrm{m}$ for Example 1: the solution with the new discrete TBC (—) coincides with the half–space solution, while the solution with the discretized TBC ($\cdots$) introduces a phase–shift and artificial oscillations.
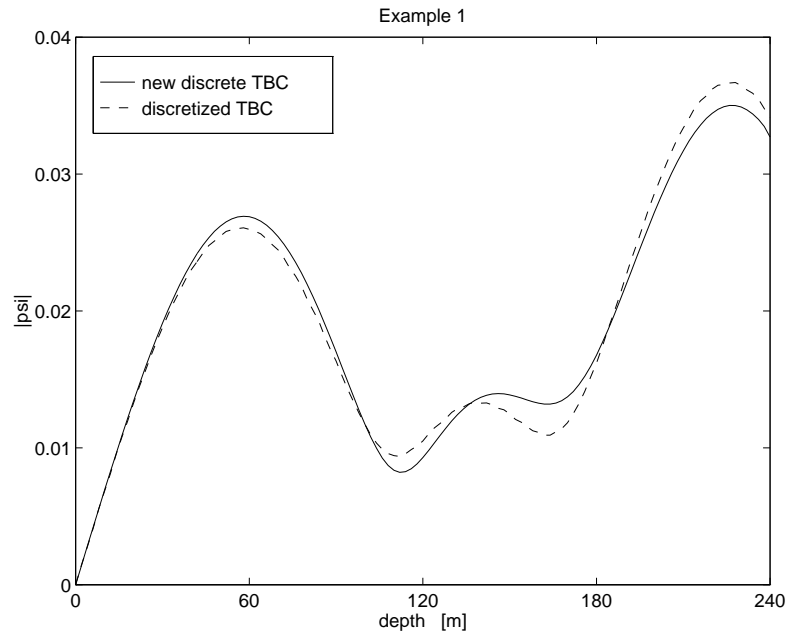

FIGURE 2. Vertical cut of the solution at $r = 19\,\mathrm{km}$ for Example 1: $|\psi(z, r = 19\,\mathrm{km})|$

The maximum range of interest is $10\,\mathrm{km}$ and the reference sound speed is chosen as $c_0 = 1500\,\mathrm{ms^{-1}}$. The calculations were carried out using the depth step $\Delta z = 0.25\,\mathrm{m}$ and the range step $\Delta r = 2.5\,\mathrm{m}$. Since the source is placed close to the bottom, the TBC was applied $10\,\mathrm{m}$ below the ocean–bottom interface (the same was done in [33]).
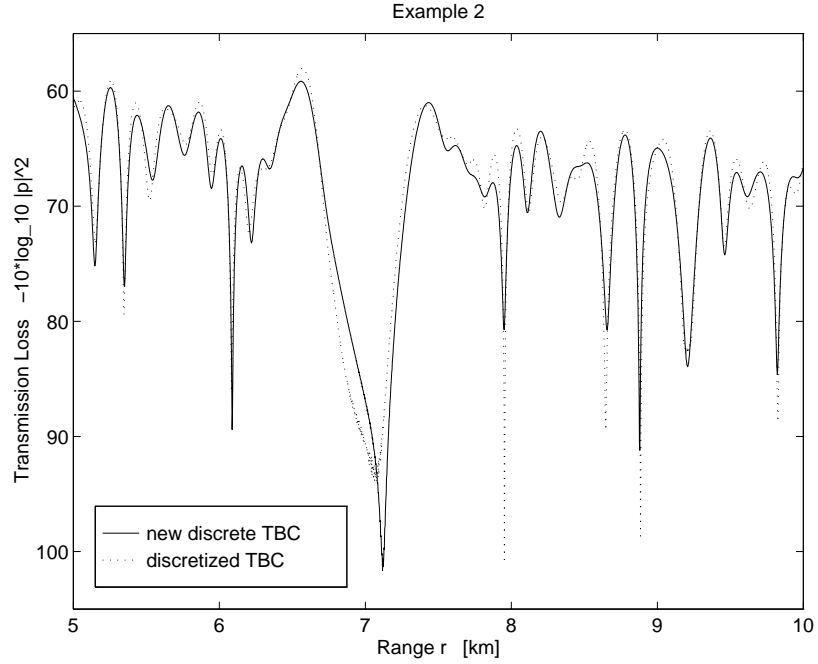

FIGURE 3. Transmission loss at $z_r = 99.5\,\mathrm{m}$ for Example 2: the solution with the new discrete TBC coincides with the half–space solution, while the solution with the discretized TBC still deviates significantly from it for the chosen discretization.
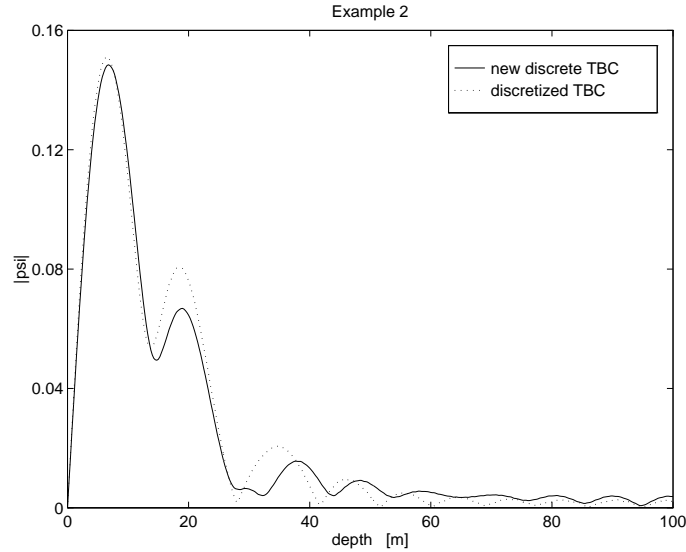

FIGURE 4. Vertical cut of the solution at $r = 7\,\mathrm{km}$ for Example 2: $|\psi(z, r = 7\,\mathrm{km})|$

The typical feature of this problem is the large destructive interference null at a range of $7\,\mathrm{km}$. Figure 3 displays the transmission loss results from 5 to $10\,\mathrm{km}$.

Figure 4 shows the deviation of the solution with the discretized TBC compared to the computed half–space solution, which coincides with the solution using our new discrete TBC.

5. Conclusions

We have derived a new discretization (*discrete TBC*) of the TBC for the WAPE of acoustics. It is of discrete convolution form involving the boundary data from the whole "past range". The convolution coefficients s_n are calculated via a simple three–term recurrence relation and they decay like $O(n^{-3/2})$. Since our new DTBC has the same convolution structure as existing discretizations, it requires the same computational effort but improves two shortcomings: DTBCs are more accurate (in fact, as accurate as the discrete half–space problem) and they yield an unconditionally stable scheme.

We point out that the superiority of DTBCs over other discretizations of TBCs is not restricted to the WAPE or to our particular interior discretization scheme (see e.g. [5, 14, 15]). Their applicability to other models only depends on the possibility to derive them explicitly; in our case the crucial point was to find the inverse Z–transformation of (3.10) explicitly. As a general philosophy, DTBCs should be used (if derivable) whenever highly accurate solutions are important.

References

[1] M. Abramowitz and I.A. Stegun, *Handbook of Mathematical Functions*, National Bureau of Standards, Applied Math. Series #55, Dover Publications, 1965.

[2] D.S. Ahluwalia and J.B. Keller, *Exact and asymptotic representations of the sound field in a stratified ocean*, in *Wave Propagation and Underwater Acoustics*, Lecture Notes in Physics 70, eds. J.B. Keller and J.S. Papadakis, Springer, New York, 1977, pp. 14–85.

[3] G.D. Akrivis, V.A. Dougalis and G.E. Zouraris, *Error Estimates for Finite Difference Methods for a Wide–Angle "Parabolic" Equation*, SIAM J. Num. Anal. **33** (1996), 2488–2509.

[4] D.E. Amos, *Algorithm 644: A Portable Package for Bessel Functions of a Complex Argument and Nonnegative Order*, ACM Trans. Math. Software **12** (1986), 265–273.

[5] A. Arnold, *Numerically Absorbing Boundary Conditions for Quantum Evolution Equations*, To appear in: *Proceedings of the "International Workshop on Computational Electronics"*, Tempe, USA, 1995; VLSI Design **63**–5 (1997).

[6] A. Arnold and M. Ehrhardt, *Discrete transparent boundary conditions for wide angle "parabolic" equations in underwater acoustics*, submitted to J. Comp. Phys., 1997.

[7] V.A. Baskakov and A.V. Popov, *Implementation of transparent boundaries for numerical solution of the Schrödinger equation*, Wave Motion **14** (1991), 123–128.

[8] *Bateman Manuscript Project*, Tables of Integral Transforms, vol. 1, McGraw–Hill, 1954.

[9] C.H. Bruneau and L. Di Menza, *Conditions aux limites transparentes et artificielles pour l'équation de Schrödinger en dimension 1 d'espace*, C. R. Acad. Sci. Paris, Ser. I **320** (1995), 89–94.

[10] J.F. Claerbout, *Coarse grid calculation of waves in inhomogeneous media with application to delineation of complicated seismic structure*, Geophysics **35** (1970), 407–418.

[11] M.D. Collins, *Applications and time–domain solution of higher–order parabolic equations in underwater acoustics*, J. Acoust. Soc. Am. **86** (1989), 1097–1102.

[12] M.D. Collins, *A higher–order parabolic equation for wave propagation in an ocean overlying an elastic bottom*, J. Acoust. Soc. Am. **86** (1989), 1459–1464.

[13] M.D. Collins, *Higher–Order and elastic parabolic equations for wave propagatiion in the ocean*, in *Computational Acoustics, vol. 3*, eds. D. Lee, A. Cakmak, and R. Vichnevetsky, Proceedings of IMACS, New Brunswick, NJ, 167–184, 1990.

[14] J. Douglas Jr., J.E. Santos, D. Sheen and L.S. Bennethum, *Frequency domain treatment of one–dimensional scalar waves*, Math. Mod. and Meth. in Appl. Sc. **3** (1993), 171–194.

[15] M. Ehrhardt, *Discrete Tranparent Boundary Conditions for Parabolic Equations*, Submitted to ZAMM, Proceedings of the GAMM Conference, 1996.

[16] L. Fishman, *Exact and operator rational approximate solutions of the Helmholtz, Weyl composition equation in underwater acoustics — The quadratic profile*, J. Math. Phys. **33** (1992), 1887–1914.

[17] R.R. Greene, *The rational approximation to the acoustic wave equation with bottom interaction*, J. Acoust. Soc. Am. **76** (1984), 1764–1773.

[18] L. Halpern and L.N. Trefethen, *Wide–angle one–way wave equations*, J. Acoust. Soc. Amer. **84** (1988), 1397–1404.

[19] J.R. Hellums and W.R. Frensley, *Non–Markovian open–system boundary conditions for the time–dependent Schrödinger equation*, Phys. Rev. B **49** (1994), 2904–2906.

[20] F.B. Jensen and W.A. Kuperman, *Consistency Tests of Acoustic Propagation Models*, SACLANTCEN Memorandum SM – **157**, 1982.

[21] D. Lee and S.T. McDaniel, *Ocean acoustic propagation by finite difference methods*, Comput. Math. Appl. **14** (1987), 305–423.

[22] D. Lee, G. Botseas and J.S. Papadakis, *Finite–difference solution to the parabolic wave equation*, J. Acoust. Soc. Am. **70** (1981), 795–800.

[23] B. Mayfield, *Non–local boundary conditions for the Schrödinger equation*, Ph.D. thesis, University of Rhode Island, Providence, RI, 1989.

[24] S.T. McDaniel and D. Lee, *A finite–difference treatment of interface conditions for the parabolic wave equation: The horizontal interface*, J. Acoust. Soc. Am. **71** (1982), 855–858.

[25] J.S. Papadakis, *Impedance formulation of the bottom boundary condition for the parabolic equation model in underwater acoustics*, NORDA Parabolic Equation Workshop, NORDA Tech. Note 143, 1982.

[26] J.S. Papadakis, M.I. Taroudakis, P.J. Papadakis and B. Mayfield, *A new method for a realistic treatment of the sea bottom in the parabolic approximation*, J. Acoust. Soc. Am. **92** (1992), 2030–2038.

[27] J.S. Papadakis, *Impedance Bottom Boundary Conditions for the Parabolic–Type Approximations in Underwater Acoustics*, in Advances in Computer Methods for Partial Differential Equations VII, eds. R. Vichnevetsky, D. Knight, and G. Richter, IMACS, New Brunswick, NJ, 1992, pp. 585–590.

[28] F. Schmidt and P. Deuflhard, *Discrete transparent boundary conditions for the numerical solution of Fresnel's equation*, Comput. Math. Appl. **29** (1995), 53–76.

[29] F. Schmidt and D. Yevick, *Discrete transparent boundary conditions for Schrödinger–type equations*, submitted to J. Comp. Phys., 1997.

[30] G. Szegö, *Orthogonal Polynomials*, Amer. Math. Soc. Colloquium Publications 23, 3rd ed. 1967.

[31] F.D. Tappert, *The parabolic approximation method*, in *Wave Propagation and Underwater Acoustics*, Lecture Notes in Physics 70, eds. J.B. Keller and J.S. Papadakis, Springer, New York, 1977, pp. 224–287.

[32] D.J. Thomson, *Wide–angle parabolic equation solutions to two range–dependent benchmark problems*, J. Acoust. Soc. Am. **87** (1990), 1514–1520.

[33] D.J. Thomson and M.E. Mayfield, *An exact Radiation Condition for Use with the A Posteriori PE Method*, J. Comp. Acous. **2** (1994), 113–132.